Available online at www.sciencedirect.com
SCIENCE DIRECT
Journal of Molecular Catalysis A: Chemical 245 (2006) 26–36
JOURNAL OF MOLECULAR CATALYSIS A: CHEMICAL
www.elsevier.com/locate/molcata

Effect of magnesium promoter on iron-based catalyst for Fischer–Tropsch synthesis

Jun Yang [a], Yuchuan Sun [a], Yu Tang [a], Ying Liu [b], Hulin Wang [b], Lei Tian [b], Hong Wang [b], Zhixin Zhang [b], Hongwei Xiang [b], Yongwang Li [b,*]

[a] *Department of Chemistry, Jinan University, Guangzhou 510632, PR China*
[b] *State Key Laboratory of Coal Conversion, Institute of Coal Chemistry, Chinese Academy of Sciences, Taiyuan 030001, PR China*

Received 5 July 2005; received in revised form 29 August 2005; accepted 30 August 2005
Available online 21 October 2005

Abstract

A series of precipitated Fe/Cu/K/SiO_2 Fischer–Tropsch synthesis (FTS) catalysts incorporated with the magnesium promoter were prepared by the combination of coprecipitation and spray-drying technology. The catalysts were characterized by using N_2 physisorption, H_2 or CO temperature-programmed reduction (TPR), X-ray diffraction (XRD), and Mössbauer spectroscopy (MES) methods. The results show that the addition of the magnesium promoter increases the BET surface area of the catalyst, and leads to the formation of the relatively smaller crystallite size of α-Fe_2O_3 in the catalysts, facilitating the reduction and carburization. The extent of carburization increases with the increase of the magnesium content, and passes through a maximum at an Mg/Fe weight ratio of 0.07. The FTS performance of the catalyst were tested in a fixed bed reactor under the conditions of 250 °C, 2.0 MPa and 2000 h^{-1} for 230 h on stream with syngas (molar ratio, $H_2/CO = 2$) used as feed gas. The results indicate that an appropriate amount of magnesium can improve the activity and stability of the catalysts, enhance the selectivity to C_5–C_{11} and increase the space time yield of C_5^+ hydrocarbon. The magnesium promoter can also slightly inhibit the activity of WGS, resulting in the decline of CO_2 selectivity and increase of the carbon utilization. However, excessive addition of the magnesium promoter will lead to a rapid deactivation of the catalyst. The optimal catalyst with Mg/Fe = 0.07 (M-3) has high activity and good stability, and keeps the selectivities of effective hydrocarbons ($C_2^=$–$C_4^=$ + C_5^+) and CH_4 at about 83% and 8%, respectively, during the entire run period.

Keywords: Magnesium promoter; Fischer–Tropsch synthesis; Iron-based catalyst; Fixed bed reactor; Spray-drying technology

1. Introduction

Fischer–Tropsch synthesis (FTS) as an alternative route for converting syngas that was derived from coal or natural gas to transportation fuels and other chemicals [1–3], has attracted much interest in recent years [4–6]. Due to the high FTS and water–gas-shift (WGS) activity, iron-based catalyst is the preferred catalyst for FTS using low H_2/CO ratio syngas from coal gasification or CO_2 reforming of natural gas [7–8].

In order to improve the catalytic performance of iron-based catalyst, researchers have studied the effects of some metal promoters, especially potassium [9–10]. Potassium addition can restrain the hydrogenation ability, suppress the formation of methane, enhance the selectivities of olefins and higher molecular weight products and facilitate the WGS reaction [11–12]. However, there is little work reported on adding magnesium as a promoter. Recently, Luo and Davis [10] compared group II alkali-earth metal-promoted iron-based catalysts with potassium-promoted and unpromoted catalysts under medium pressure conditions appropriate for slurry reactor operations. The results showed that the catalysts promoted with magnesium have lower FTS activity and lower chain growth factor than the potassium-promoted iron catalyst, but higher activity and chain growth factor than an unpromoted catalyst. In addition, it was found that the magnesium promoter has a negative effect on WGS activity. Gallegos et al. [13] investigated the Fe/SiO_2-MgO catalysts for FTS reaction. The experimental results showed that the rate of total hydrocarbon formation increased with the increase of the MgO content, and that the optimal content of MgO could increase the selectivity to olefins

* Corresponding author. Tel.: +86 351 413 0337; fax: +86 351 413 0337.
E-mail address: ywl@sxicc.ac.cn (Y. Li).

1381-1169/$ – see front matter © 2005 Elsevier B.V. All rights reserved.
doi:10.1016/j.molcata.2005.08.051

and suppress the formation of CH_4. The catalysts were characterized by using selective chemisorption of CO, O_2 volumetric oxidation and Mössbauer spectroscopy (MES). The results indicated that MgO concentrated the surface of SiO_2 and could modify the metal crystal size. Dry and Oosthuizen [14] studied the role of alkali earth metals on the chemisorption heat of syngas on the surface of a promoted iron FTS catalyst. The results showed that the MgO promoter did not significantly change the heat of adsorption for any gas and acted purely as a structural promoter. Dutartre et al. [15] studied the activation of H_2 over an Fe/MgO catalysts with the helps of Mössbauer spectroscopy and magnetic techniques. Putanov et al. [16] studied the effects of MgC_2O_4 (prepared from magnesium nitrate and magnesium acetate) as a support precursor on the properties of iron/magnesium catalysts. Their results indicated that the catalyst with the support prepared from magnesium nitrate had the higher activity by one order of magnitude than that from magnesium acetate, but the catalyst with the support prepared from magnesium acetate showed better initial selectivity toward alkenes and a lower initial deactivation than that from magnesium nitrate. However, these previous studies did not give a detailed explanation about the effects of the group II alkali-earth metals on the performance of an iron-based catalyst.

This paper aims at a systematic understanding of the effect of the magnesium promoter on precipitated Fe/Cu/K/SiO_2 catalysts under industrially relevant operation conditions. Particular attention is focused on the effect of magnesium on the catalyst activation, on the textural properties and on the bulk phase structures of the fresh, activated and used catalysts. The FTS and WGS activity, olefin and oxygenate selectivity, and hydrocarbon product distribution are correlated with the catalyst characterization results.

2. Experimental

2.1. Catalyst preparation

Mg-promoted Fe/Cu/K/SiO_2 catalysts used in this study were prepared by a combination of co-precipitated and spray-dried method. A solution containing $Fe(NO_3)_3{\cdot}9H_2O$, $Cu(NO_3)_2{\cdot}2H_2O$ and $Mg(NO_3)_2{\cdot}6H_2O$ in the desired ratio was added to a continuously stirred tanker together with a sodium carbonate solution. When the slurry pH value was maintained at 7–7.5, a precipitate was obtained. The precipitate was washed completely with deionized water, subsequently filtered. The final cake was reslurried in deionized water. The potassium silicate was added in rigorous stirring. Then the slurry was spray dried at 250 °C in a QZR-5 spray drier (Linzhou Spray Dryer Co., PR China) in air, and the spray-dried powder as prepared was calcined at 320 °C for 5 h in a muffle furnace. The fresh catalysts exhibit good micrometer-scale spherical particles with an average size of 23 μm. The compositions of the five catalysts are 100Fe/5Cu/6K/xMg/20SiO_2 (x = 0, 2, 4, 7, 11). Which were labeled as M-0, M-1, M-2, M-3 and M-4, respectively. The detailed preparation method can be found elsewhere [17]. In all tests, the catalysts were pressed into particles, crushed and sieved to retain 20–40 mesh particles prior to loading to a fixed bed reactor.

2.2. Catalyst characterization equipments and methods

BET surface area, pore volume and average pore diameter of the fresh and activated catalysts were measured by N_2 physisorption at −196 °C using a Micromeritics ASAP 2500 system. Samples were degassed at 120 °C for 6 h prior to measurement.

Temperature-programmed reduction (TPR) studies were performed using a mixture gas of 5% H_2/95% Ar (H_2-TPR) or 5% CO/95% He (CO-TPR). In H_2-TPR experiment, about 40 mg of catalyst was packed in an atmospheric quartz tube flow reactor (5 mm i.d.). Then the catalyst sample was heated in a flow of 5% H_2/95% Ar from room temperature to 800 °C at a heating rate of 6 °C/min, and the flow rate of the reduction gas was 40 ml/min in the standard state. Hydrogen consumption was monitored by the change of thermal conductivity of the effluent gas stream. The conditions of CO-TPR experiment are similar to those for H_2-TPR, and the only difference is that a liquefied nitrogen bath was used to remove CO_2 formed during the carbon monoxide reduction.

Powder X-ray diffraction (XRD) patterns of the catalyst samples were determined on a D/max-RA X-ray diffractometer (Rigaku, Japan) with Cu Kα radiation (λ = 0.154 nm), operated at 40 kV and 100 mA. Standard powder XRD cards, compiled by the Joint Committee on Powder Diffraction Standards (JCPDS) and published by the International Center for Diffraction Data, were used to identify the iron phase of the fresh, activated and used catalysts. The Mössbauer spectra of catalysts were recorded at room temperature by using a CANBERRA Series 40 MCA constant-acceleration Mössbauer spectrometer (CANBERRA, USA). The γ-ray source was ^{57}Co/Pd. All spectra were analyzed with a non-linear least squares fitting routine that models the spectra as a combination of singlets, quadruple doublets and magnetic sextuplets based on a Lorentzian line shape profile. Magnetic hyperfine fields were calibrated with the field of α-Fe at room temperature. The hyperfine parameters, the isomer shift (IS), the quadruple splitting (QS), and the magnetic hyperfine field (Hhf), were used to identify the spectral components. Usually it was assumed that the Mössbauer area ratios are equal to a relative amount of the associated species.

2.3. Reactor system and operating procedures

The catalytic performances of the catalysts for FTS were conducted in a stainless steel fixed bed reactor with an internal diameter of 12 mm and an effective bed length of approximately 15 cm. The feed gas with H_2/CO ratio of about 2.0 was prepared by the decomposition of methanol. Prior to entering the reactor, the feed gas passed through a series of columns (a sulfur-removal trap, an oxygen-removal trap, an activated charcoal trap and a silica-gel/5A molecular sieve trap) to remove tiny amounts of sulfur, oxygen, carbonyls and water. The flow rate of the purified syngas was adjusted with a mass flow controller. After leaving the reactor, the stream passed through a hot trap (130 °C,

collecting the high molecular weight hydrocarbons) and a cold trap (0 °C, collecting the liquid products) at the system pressure. After the product collectors, the pressure was released through a backpressure regulator. The flow rate of the tail gas was monitored by a wet-gas flow meter. A detailed description of the reactor system used in this study was introduced elsewhere [18,26].

In FTS reaction experiments, 5 ml of the catalyst was packed in the reactor and then activated for 15 h using syngas with an H_2/CO ratio of 2.0 under the conditions of 250 °C, 0.25 MPa and 1000 h^{-1}. After activation, the reactor temperature was cooled to 150 °C, and then the reactor system was adjusted to desired pressure and space velocity. The temperature was gradually increased to 250 °C within 7 h. During the whole reaction period, the products in the hot and cold traps are collected usually with the intervals of about 12 h.

The products of FTS and the feed gas were all analyzed off-line using gas chromatographs (GC). H_2, CO and CH_4 were separated on a GC 920 (Shanghai Analyzer Co., China) with a 13× molecular sieve packed column (1.5 m × 3 mm i.d., Ar carrier), and then they were analyzed using a thermal conductivity detector (TCD). C_1–C_8 hydrocarbons in the tail gas were analyzed on a Shimadzu-7A GC equipped with a modified Al_2O_3 packed column (1.5 m × 3 mm i.d., N_2 carrier) and a flame ionization detector (FID). The oil phase collected in the cold trap was analyzed on an Agilent 6890N (Agilent, HP) gas chromatograph using a DB-1 quartz capillary column (60 m × 0.25 mm i.d., N_2 carrier) and an FID under temperature programming, and oxygenates in the water phase were measured by an Agilent 6890N gas chromatograph with a DB-WAX quartz capillary column (30 m × 0.32 mm i.d., FID, H_2 carrier). Wax collected in the hot trap was analyzed on a GC 920 with a UA^+-(HT) stainless capillary column (30 m × 0.53 mm i.d., N_2 carrier) and an FID under temperature programming. A GC 920 with a packed column (401, 1 m × 3 mm i.d., H_2 carrier) and TCD were used to analyze the amount of CO_2 in the tail gas. The CO_2 concentration was calculated by the external standard method.

2.4. Catalyst activation

The catalyst samples used for XRD and MES characterization were activated in a quartz tube under the same conditions (250 °C, 0.25 MPa, $H_2/CO = 2$ and 1000 h^{-1}) for 15 h. After activation, the quartz tube was cooled to room temperature and sealed in an inert atmosphere. Then the quartz tube was transferred to a glove box with Ar protection, in which the reduced samples were transferred to glass tubes and coated with paraffin wax for preventing the oxidation and then sealed for characterization of XRD and MES. The catalysts for the characterization of BET were reduced under above conditions. The reduced catalysts were washed several times with xylene, and protected with absolute ethanol for characterization.

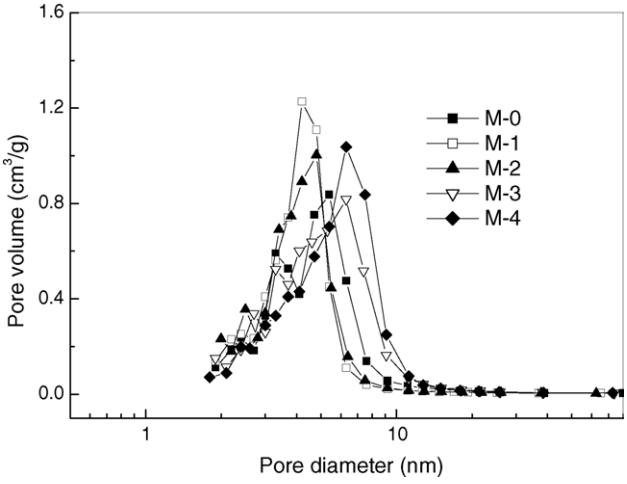

Fig. 1. Pore size distribution of the fresh catalysts with different magnesium contents.

3. Results and discussion

3.1. Textural properties of the fresh and activated catalysts

Textural properties and pore size distributions of the fresh iron-based catalysts with different magnesium contents are shown in Table 1 and Fig. 1, respectively. It can clearly be seen that the addition of the magnesium promoter significantly improves the BET surface area of the fresh catalysts (Table 1). However, in the experimental range of Mg/Fe mass ratio (0.02–0.11), the BET surface area of the fresh catalysts monotonously declines with the increase of the magnesium content. As shown in Table 1 and Fig. 1, the pore size distribution of the fresh catalysts without the magnesium promoter or with higher magnesium content show a shoulder peak, but those of the catalysts with lower content of the magnesium promoter only show a single peak.

Textural properties of the activated catalysts are summarized in Table 2. Compared with Table 1, one can see that, after the activation, the BET surface areas and the pore volumes of the activated catalysts significantly decrease, and that the pore diameters significantly increase. The BET surface areas of the all activated catalysts are in the range of 81–90 m^2/g and there is

Table 1
Textural properties of the fresh catalysts with different magnesium contents

Catalysts	Mg/Fe (wt/wt)	BET (m^2/g)	Pore volume (cm^3/g)	Maximal probability pore diameter (nm)
M-0	0	214	0.27	3.5, 5.5
M-1	0.02	250	0.28	4.5
M-2	0.04	246	0.27	4.5
M-3	0.07	237	0.33	3.5, 6.0
M-4	0.11	230	0.36	3.5, 6.5

Table 2
Textural properties of the activated catalysts with different magnesium contents

Catalysts	Mg/Fe (wt/wt)	BET (m^2/g)	Pore volume (cm^3/g)	Maximal probability pore diameter (nm)
M-0	0	82	0.22	7.3
M-1	0.02	84	0.19	6.0
M-2	0.04	89	0.21	6.0
M-3	0.07	86	0.23	7.0
M-4	0.11	91	0.27	7.3

no clear correlation between the BET surface areas of the activated catalysts and the magnesium promoter content. The pore size distributions of the activated catalysts show single peaks. It is clearly seen that the distributions of small pores with diameter less than 3.5 nm of catalysts significantly decrease, and that the maximal probability pore diameter significantly increases (from 3–4 nm to 6–7 nm) after activation. The probable reason is that the smaller pores collapse forming bigger pores during the activation process. Similar results over iron-based catalysts have also been reported by other researchers [19–21].

3.2. Temperature-programmed reduction

The effects of the magnesium promoter on the reduction behavior of the catalysts were measured by H_2-TPR and CO-TPR. The profiles of H_2-TPR and CO-TPR are presented in Figs. 2 and 3, respectively. As shown in Fig. 2, all catalysts present two main reduction peaks at about 300 °C and 550 °C in the H_2-TPR profiles. It has been postulated that the first stage corresponds to the reductions of α-Fe_2O_3 to magnetite (Fe_3O_4) and CuO to Cu, whereas the second stage corresponds to subsequent reduction of Fe_3O_4 to metallic iron (α-Fe) [8]. It is also found that the first stage can be further separated into two peaks, the first peak corresponds to the reduction of the solid solution of CuO and part of α-Fe_2O_3 to Cu and Fe_3O_4 [8], and the second small peak is ascribed to the reduction of the residual α-Fe_2O_3 to Fe_3O_4. The profiles clearly show that the first reduction peaks of catalysts shifts to lower temperature with the increasing of the magnesium content, except for the catalyst M-4 with the highest magnesium content (Mg/Fe = 0.11). This suggests that the addition of the magnesium promoter enhances the reduction of α-Fe_2O_3 in H_2 and which results in a decrease in the reduction temperature. For the catalysts with lower magnesium content, namely M-0, M-1 and M-2, the area of the first small reduction peak (ca. 300 °C) increases with the increase of the magnesium content. Such results indicate that the addition of small amount of magnesium promotes the dispersion of Cu promoter, improving the reduction of α-Fe_2O_3 that interacts with the Cu promoter. However, for the catalysts M-3 and M-4 with higher magnesium content, the area of the first small reduction peak declines, especially for M-4, the first smaller reduction peak almost disappears. Meanwhile, the second small reduction peak significantly increases and the reduction temperature shifts to higher temperature with the increase of the magnesium content. The probable reason is that small amount of magnesium promoter can promote the dispersion of Cu promoter which enhances the effect of Cu promoter and improve the reduction of the catalyst, and the excessive Mg promoter may weaken the interaction between Cu and Fe oxide and results in a restraint of the catalyst reduction.

As shown in Fig. 2, the reduction temperature of the second stage (the reduction of Fe_3O_4 to α-Fe) of the Mg-promoted catalysts promoter shifts to higher temperature. This may be due

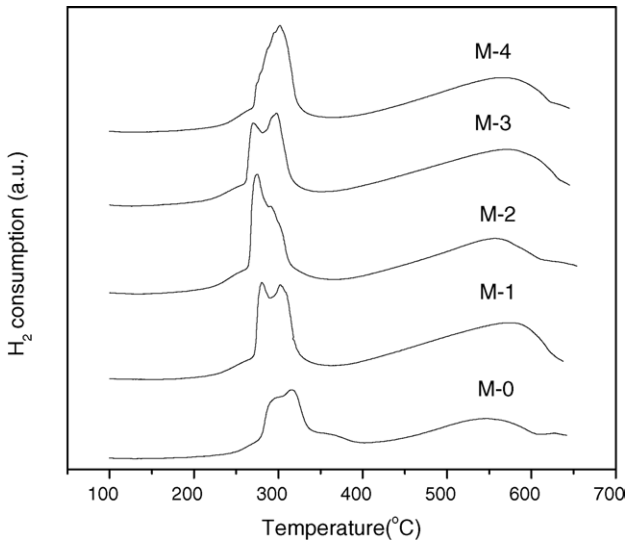

Fig. 2. H_2-TPR profiles of the fresh catalysts with different magnesium contents.

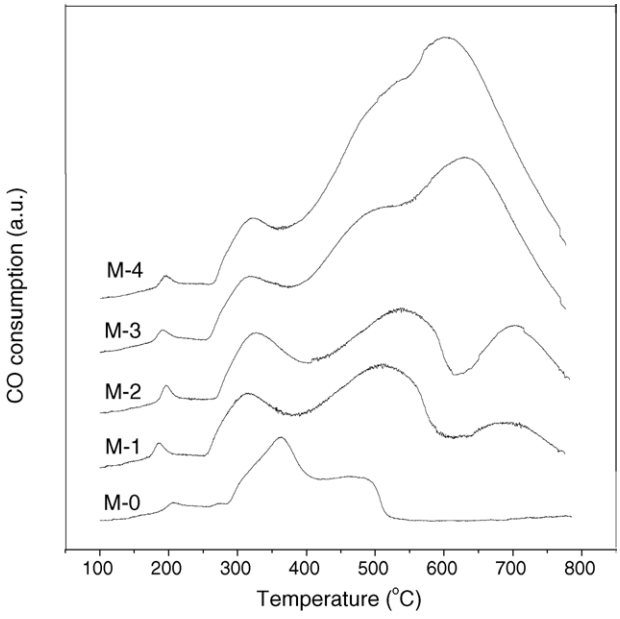

Fig. 3. CO-TPR profiles of the fresh catalysts with different magnesium contents.

to the formation of a solid solution of Fe_3O_4 and MgO that is difficult to be reduced during the course of the TPR at higher temperature. However, the effect of the magnesium content on the reduction temperature of this stage is not clear.

The effects of the magnesium content on CO-TPR of the catalysts are shown in Fig. 3. It is found that all the five catalysts show four-peak patterns. For the catalyst without the magnesium promoter, M-0, the area of the first small peak (ca. 200 °C) is bigger than the area of the second small peak (ca. 280 °C). The first peak is probably attributed to the reduction of the solid solution of CuO and α-Fe_2O_3 to Cu and Fe_3O_4, and the second small peak is attributed to the reduction of α-Fe_2O_3 to Fe_3O_4 [8]. In contrast to this, the magnesium-promoted catalysts present only one small peak below 300 °C and the area of the first small peak (ca. 200 °C) is bigger than that of the catalyst M-0. These results suggest that a certain content of magnesium can promote the dispersion of CuO, strengthen the interaction of CuO and α-Fe_2O_3 and improve the reduction of α-Fe_2O_3. The results are consistent with those observed in H_2-TPR (Fig. 2). According to the literature [8], the other two reduction peaks (ca. 360 °C and 490 °C) of the catalyst M-0 may correspond to the transformation of Fe_3O_4 to iron carbide (χ-carbides) and the inter-transformation (χ-carbides to cementite) among various iron carbides, since cementite is the stable carbide phase at high temperature. The magnesium-promoted catalysts present three reduction peaks at temperatures of ca. 320 °C, 530 °C and 600–700 °C, respectively. It can be seen that, for the magnesium-promoted catalysts, the peak of ca. 320 °C corresponding to the reduction of magnetite to χ-carbide shifts to the lower temperature which indicates that the addition of the magnesium can facilitate the carburization of the catalysts. It is well-known that the Boudouard reaction ($2CO \rightarrow C + CO_2$) which leads to the carbon deposition usually accompanies the phase transformations during the reduction process of the catalysts. Recently, Jin and Datye [8] studied the Fe/Cu/SiO_2 catalyst and found that the carbon deposition occurs in parallel with carbide formation, no carbon deposition being observed in the catalyst that was not carburized. From Fig. 3, it is found that there is no peak in the pattern of the catalyst without the magnesium promoter over 500 °C, whereas the magnesium-promoted catalysts present a bigger peak in the range of 600–700 °C, especially for the catalyst with higher Mg content (M-3 and M-4). This is probably due to the carbon deposition. This difference strongly suggests that the magnesium can promote the carburization of the catalysts, leading to a significant carbon deposition during reduction.

3.3. Bulk phase structure

XRD and Mössbauer spectroscopy are used to detect the bulk phases of the fresh, reduced and used catalysts.

3.3.1. Catalysts as prepared

The XRD patterns of the fresh catalysts are shown in Fig. 4. For the catalyst M-0, the only detectable phase is α-Fe_2O_3, which has characteristic diffraction peaks at 2θ values of 24.3°, 33.3°, 35.8°, 40.9°, 49.6°, 54.2°, 57.6° and 64.1°. With the incorporation of the magnesium promoter, the characteristic peaks of

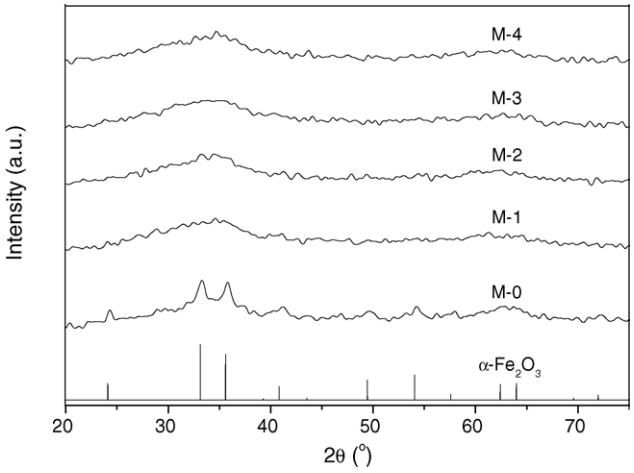

Fig. 4. XRD patterns for the fresh catalysts with different magnesium contents.

α-Fe_2O_3 in the fresh catalysts were weakened, and only two broad diffraction regions appeared. Such results indicate that addition of magnesium into the catalyst can promote the dispersion of α-Fe_2O_3 crystallite, which is consistent with the results of the BET surface area mentioned above. No characteristic signals of MgO can be observed in the X-ray diffraction patterns, it imply that MgO is well dispersed in the catalysts.

The Mössbauer parameters of the fresh catalysts are summarized in Table 3. The MES spectra of the catalyst M-0 include a sextet and a doublet, whereas the MES spectra of the magnesium promoted catalysts include only a doublet. According to the MES parameters listed in Table 3, the sextet is assigned to the magnetic α-Fe_2O_3 with crystallites size larger than 13.5 nm [22–24]. The doublet is typical for the superparamagnetic (spm) Fe^{3+} ions on the non-cubic sites [23]. The catalyst M-0 consists of 26.5% ferromagnetic α-Fe_2O_3 and 73.5% Fe^{3+} (spm) and all the magnesium-promoted catalysts are composed of 100% Fe^{3+} (spm). The results indicate that the magnesium promoter can enhance the dispersion of the α-Fe_2O_3 phase. These results are well consistent with the results of BET and XRD characterization. Gallegos et al. [13] studied the Fe/SiO_2/MgO catalysts for FTS by selective chemisorption of CO, volumetric oxidation and MES, and found that MgO covers on the surface of SiO_2 and modifies the metallic crystal size; it is well agree with our results.

3.3.2. Activated catalysts

The XRD patterns of the catalysts with different levels of magnesium after being activated with syngas ($H_2/CO = 2.0$) at 250 °C, 0.25 MPa and 1000 h^{-1} for 15 h are presented in Fig. 5. The XRD pattern of the catalyst M-0 shows the characteristic peaks of α-Fe_2O_3 at 2θ values of 33.1°, 35.6°, 54, 62.5° and 64°, and no Fe_3O_4 and iron carbides can be detected by XRD. The XRD patterns of the catalysts promoted with magnesium show a broad peak centered at 43°. According to the Data of JCPDS, since most iron carbides have the characteristic peaks at about 43°, the broad diffraction region may be attributed to iron carbides or the overlap of Fe_3O_4 and iron carbides. It is also found that the peak intensity increases with the increase of the

Table 3
Mössbauer parameters of the fresh catalysts with different magnesium contents

Catalysts	Phases	Mössbauer parameters			Spectral contribution (%)
		IS (mm/s)	QS (mm/s)	Hhf (kOe)	
M-0	α-Fe_2O_3	0.35	−0.24	490	26.5
	Fe^{3+} (spm)	0.33	0.78	–	73.5
M-1	Fe^{3+} (spm)	0.33	0.83	–	100.0
M-2	Fe^{3+} (spm)	0.34	0.80	–	100.0
M-3	Fe^{3+} (spm)	0.33	0.83	–	100.0
M-4	Fe^{3+} (spm)	0.33	0.82	–	100.0

magnesium content and reaches a maximum at the Mg/Fe = 0.07 (M-3). Beyond this content, the intensity of the diffraction peaks declines. These results suggest that the catalysts get easy to be reduced and carburized with the increase of the magnesium content when the Mg/Fe mass ratio is below 0.11, however, the excessive addition of the magnesium promoter will suppress the reduction and carburization. This is consistent with the results of H_2-TPR and CO-TPR.

The Mössbauer parameters of the activated catalysts are presented in Table 4. The Mössbauer spectrum of the catalyst M-0 show three sextets and two doublets. However, for the catalysts promoted with magnesium, M-1 has only two doublets, M-2 and M-4 have one sextet and two doublets and M-3 has three sextets and two doublets. According to the spectral parameters summarized in Table 4, the values of the sextet with isomer shift of 0.35 mm/s, quadruple splitting of 0.01 mm/s and hyperfine field of 490 kOe imply the presence of α-Fe_2O_3. The sextets with Hhf of 465 kOe and 425 kOe can be attributed to the tetrahedral (A site) and octahedral sites (B site) of Fe_3O_4, respectively [25–26]. The doublets with isomer shift of 0.68–0.97 mm/s and quadruple splitting of 1.69–2.13 mm/s are attributed to Fe^{2+} ions in superparamagnetic state, and the doublets with isomer shift of 0.33–0.38 mm/s, quadruple splitting of 0.71–0.80 mm/s are attributed to Fe^{3+} ions in superparamagnetic state. The values of the sextets with IS of 0.26–0.34 mm/s, 0.3–0.39 mm/s and 0.27–0.43 mm/s, Hhf of 181–187 kOe, 219–225 kOe and 104–116 kOe can be attributed to I, II and III site of χ-Fe_5C_2, respectively. As shown in Table 4, there is no Fe_3O_4 in the bulk phases of the activated catalysts with the magnesium promoter and no iron carbide in the bulk phases of the catalysts M-0 and M-1. The content of the iron carbide in the catalysts with the magnesium promoter increases with the increase of the magnesium content and reaches a maximum at the content of Mg/Fe = 0.07 (M-3). After the maximum point, the content of iron carbide declines with the increase of the magnesium content. These results indicate that an optimal amount of magnesium can promote the carburization of the iron-based catalysts. And the extent of reduction increases with the increase of the magnesium content and reaches a maximum at the Mg/Fe = 0.07, then declines with further increase in the magnesium content. The CO-TPR pattern shows that the CO consumption of the catalyst M-4 is the biggest one among the five catalysts, but the MES result of the catalyst M-4 shows that the content of the iron carbide is lower than that of M-3. This suggests that there is significant carbon deposition on the catalyst M-4. The MES results obtained agree well with those of H_2-TPR, CO-TPR and XRD.

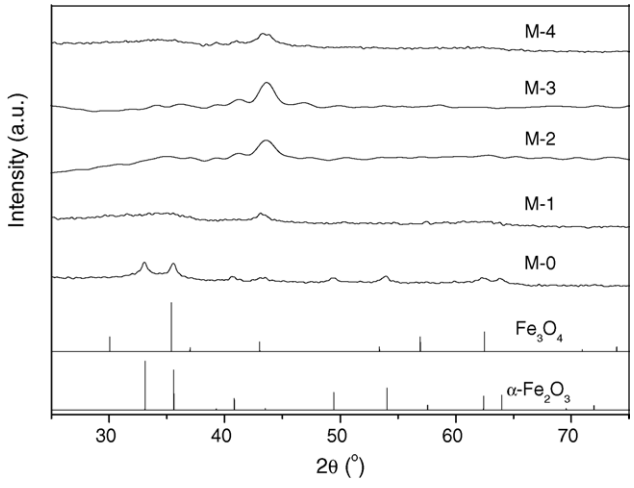

Fig. 5. XRD patterns for the reduced catalysts with different magnesium contents. Reduction conditions: $H_2/CO = 2$, 250 °C, 0.25 MPa and 1000 h^{-1} for 15 h.

3.3.3. Used catalysts

The XRD patterns of the catalysts after FTS reaction with syngas ($H_2/CO = 2.0$) at 250 °C, 2.0 MPa and 2000 h^{-1} for 230 h are presented in Fig. 6, and the Mössbauer spectra parameters are summarized in Table 5. As shown in Fig. 6, the XRD patterns of the five catalysts are similar to each other. There are a big and broad peak at 43.5° and two weak and broad diffraction regions at the range of 39–42° in the patterns. According to the data reported in the JCPDS database and in the literature [28], most of the carbide phases have prominent peaks at 31° and 43°. Therefore, the peaks at 39–42° and 43.5° may be assigned to the presence of iron carbides. Due to the poor crystallographic form of iron carbides, it is impossible to specify which carbide is obtained under these conditions or to determine the stoichiometry of those carbides from the XRD patterns.

The Mössbauer spectra of the catalysts after reaction can be fitted by three sextets and two doublets. No sextets of Fe_3O_4 are found in the patterns any of the catalysts. Huang et al. [27], Shroff et al. [28] and Bian et al. [29] reported that Fe_3O_4 is the only phase in the used iron-based catalysts by XRD analysis, which is different from the results of the present study. By comparing the analysis of the used catalysts with that of the

Table 4
Mössbauer parameters of the activated catalysts with different magnesium contents

Catalysts	Phases	Mössbauer parameters			Spectral contribution (%)
		IS (mm/s)	QS (mm/s)	Hhf (kOe)	
M-0	α-Fe_3O_2	0.35	0.01	490	21.9
	Fe_3O_4 (A)	0.41	0.04	465	2.6
	Fe_3O_4 (B)	0.75	−0.04	425	5.7
	Fe^{2+} (spm)	0.97	1.86	–	34.2
	Fe^{3+} (spm)	0.37	0.74	–	35.5
M-1	Fe^{2+} (spm)	0.97	1.69	–	56.3
	Fe^{3+} (spm)	0.35	0.80	–	43.7
M-2	χ-Fe_5C_2	0.29	0.01	189	36.2
	Fe^{2+} (spm)	0.77	1.76	–	23.9
	Fe^{3+} (spm)	0.39	0.73	–	39.9
M-3	χ-Fe_5C_2 (I)	0.26	−0.03	182	31.8
	χ-Fe_5C_2 (II)	0.31	−0.03	221	26.7
	χ-Fe_5C_2 (III)	0.27	0.19	107	19.0
	Fe^{2+} (spm)	0.68	2.13	–	6.9
	Fe^{3+} (spm)	0.33	0.72	–	15.6
M-4	χ-Fe_5C_2	0.29	−0.06	189	25.8
	Fe^{2+} (spm)	0.97	1.75	–	37.7
	Fe^{3+} (spm)	0.37	0.80	–	36.5

Activation conditions: $H_2/CO = 2$, 250 °C, 0.25 MPa and 1000 h^{-1} for 15 h.

Table 5
Mössbauer parameters of the used catalysts with different magnesium contents

Catalysts	Phases	Mössbauer parameters			Spectral contribution (%)
		IS (mm/s)	QS (mm/s)	Hhf (kOe)	
M-0	χ-Fe_5C_2 (I)	0.26	−0.05	181	28.6
	χ-Fe_5C_2 (II)	0.31	−0.01	220	24.7
	χ-Fe_5C_2 (III)	0.27	0.09	110	17.0
	Fe^{2+} (spm)	0.72	2.10	–	5.4
	Fe^{3+} (spm)	0.37	0.87	–	24.3
M-1	χ-Fe_5C_2 (I)	0.26	−0.10	184	25.4
	χ-Fe_5C_2 (II)	0.31	−0.07	222	20.5
	χ-Fe_5C_2 (III)	0.27	0.00	116	30.2
	Fe^{2+} (spm)	0.73	2.16	–	3.8
	Fe^{3+} (spm)	0.34	0.8	–	20.2
M-2	χ-Fe_5C_2 (I)	0.26	−0.10	183	28.0
	χ-Fe_5C_2 (II)	0.31	−0.05	220	28.4
	χ-Fe_5C_2 (III)	0.27	0.01	112	18.9
	Fe^{2+} (spm)	0.74	2.11	–	4.8
	Fe^{3+} (spm)	0.33	0.85	–	19.9
M-3	χ-Fe_5C_2 (I)	0.26	−0.05	182	30.1
	χ-Fe_5C_2 (II)	0.31	−0.02	221	26.8
	χ-Fe_5C_2 (III)	0.27	0.12	110	19.0
	Fe^{2+} (spm)	0.73	2.07	–	6.0
	Fe^{3+} (spm)	0.32	0.90	–	18.1
M-4	χ-Fe_5C_2 (I)	0.26	−0.07	180	32.2
	χ-Fe_5C_2 (II)	0.31	−0.04	220	26.9
	χ-Fe_5C_2 (III)	0.27	0.09	112	14.8
	Fe^{2+} (spm)	0.70	2.17	–	6.4
	Fe^{3+} (spm)	0.31	0.77	–	19.6

Reaction conditions: $H_2/CO = 2$, $T = 250$ °C, $P = 2.0$ MPa and GHSV = 2000 h^{-1} for 230 h.

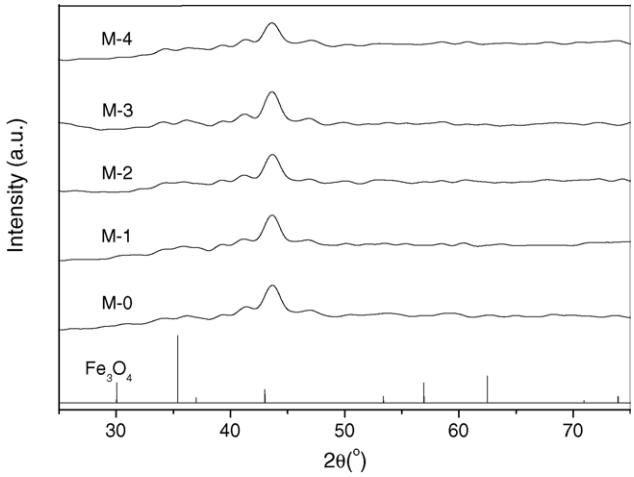

Fig. 6. XRD patterns for the used catalysts with different magnesium contents. Reaction conditions: $H_2/CO = 2$, $T = 250\,^{\circ}C$, $P = 2.0$ MPa and GHSV = 2000 h^{-1} for 230 h.

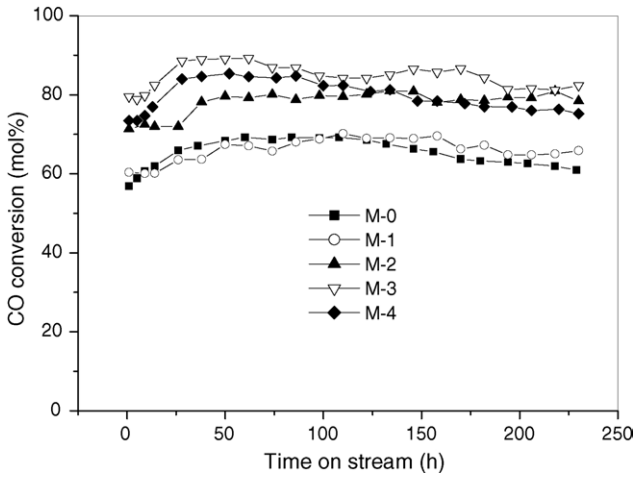

Fig. 7. CO conversion and stability of the catalysts with different magnesium contents. Reaction conditions: $H_2/CO = 2$, $T = 250\,^{\circ}C$, $P = 2.0$ MPa and GHSV = 2000 h^{-1}.

activated catalysts, one can find that Fe_3O_4 in the bulk phase of the catalyst M-0 has disappeared. For the catalysts M-0, M-1, M-2, M-4, the amounts of Fe^{2+} and Fe^{3+} ion in the superparamagnetic state decrease markedly and the amount of χ-Fe_5C_2 increases significantly, whereas the phase composition of catalysts M-3 has no obvious change. Such results suggest that all the reduced catalysts except for M-3 are far from complete reduction and carburization and can be further reduced and carburized during the FTS reaction process. As shown in Table 5, for all the used catalysts, the contents of iron carbides are similar to each other, ca. 70%, after the reaction of 230 h. The above mentioned analysis showed that an optimal amount of magnesium can accelerate the carburization of the catalysts during the reduction process, however, after a long time reaction, the extents of carburization of the catalysts will tend to become similar.

3.4. Activity and stability

The influence of the magnesium content on CO conversion of the catalysts is shown in Fig. 7. The activities in the tests firstly increase with time on stream (TOS), then reach the maximal CO conversion after about 50 h on stream, and subsequently either stabilize (catalyst M-1, M-2 and M-3) or decline (catalyst M-0 and M-4) with TOS. The CO conversions of the catalyst M-1 with Mg/Fe weight ratio of 0.02 is similar to that of the unpromoted catalyst. When the Mg/Fe weight ratio is higher than 0.02, the CO conversion of the catalysts increases significantly with the increase of the magnesium content and passes through a maximum at the Mg/Fe = 0.07 (M-3). Beyond this magnesium concentration, a decrease in catalyst activity is observed. There is a clear correlation between the carburization extent and the catalytic activity; the higher extent of carburization in the catalyst the higher CO conversion. Many studies have been devoted to the investigation of the active phase for FTS reaction [30–35], however, the controversy still remains. Riedel et al. [4] studied the Fe-Al-Cu-K_2O catalyst for Fischer–Tropsch synthesis, they found that time on stream (TOS) had dominant influence on composition and structure of the catalyst, and concluded that the reduced fresh catalyst has "no" Fischer–Tropsch activity. It will take several episodes for catalyst to construct the actual catalytic phase and reach the steady-state. They proposed that Fischer–Tropsch activity of catalyst was generated with time, when the α-Fe reacted with carbon from CO dissociation and quantitatively consumed the iron for iron carbide (particularly Fe_5C_2) formation. Thus, they suggested that iron carbide surface in its "actual state during synthesis" is the "true Fischer–Tropsch catalyst". These results in our work are consistent with that obtained by Riedel et al. [4]. Similar results also are obtained by Motjope and co-workers [34] and Mansker and co-workers [35]. It is also found that the initial activities of the catalyst M-0 and M-1 are nearly the same, but the catalyst M-1 has better stability. In order to obtain a quantitative comparison of the stability of the catalyst, the deactivated rates of the catalysts are calculated. We calculated the deactivated rates of the five catalysts. The deactivation rates of the catalysts M-0 to M-4 are 0.99%/d, 0.21%/d, 0.08%/d, 0.91%/d, and 1.37%/d, respectively. The deactivated rate of the catalysts firstly declined with the increase of the magnesium content and then reaches a minimum at the Mg/Fe = 0.04. Beyond this ratio of Mg/Fe, a monotonic increase in the deactivated rate of the catalysts is observed with the further increase of the magnesium content.

3.5. Product selectivity

Typical data of FTS activity, CO_2 selectivity and hydrocarbon distribution of the catalysts are summarized in Table 6. The CH_4 selectivity of the five catalysts is in the range of 5.5–8.5% and there is no clear correlation between the CH_4 selectivity and the magnesium content. Table 6 shows that the effect of magnesium content on olefin selectivity is significant. The olefin ($C_2^=$–$C_4^=$ and $C_5^=$–$C_{11}^=$) selectivity of catalyst M-1 with Mg/Fe weight ratio of 0.02 is lower than that of unpromoted catalyst. However, the olefin ($C_2^=$–$C_4^=$ and $C_5^=$–$C_{11}^=$) selectivity of the catalysts with magnesium promoter increases with the increase of the magnesium content and reaches a maximum at the Mg/Fe ratio of 0.07. Above this magnesium content, a decrease in the

Table 6
FTS performances of the catalysts with different magnesium contents

	Catalysts									
	M-0		M-1		M-2		M-3		M-4	
	84[a]	229[a]	86[a]	230[a]	86[a]	230[a]	86[a]	230[a]	86[a]	230[a]
CO conversion (mol%)	69.25	60.99	68.03	65.89	79.79	78.64	86.80	82.34	84.78	75.17
H_2 conversion (mol%)	30.38	26.42	28.14	29.80	37.23	37.37	42.91	39.21	36.53	32.56
CO + H_2 conversion (mol%)	44.41	36.12	41.89	42.25	51.40	51.11	57.34	53.39	52.50	40.33
$(H_2/CO)_{UR}$[b]	0.93	0.94	0.79	0.85	0.93	0.95	1.01	0.97	0.87	0.85
$(H_2/CO)_{TG}$[c]	4.43	4.91	4.35	3.91	6.22	5.87	8.83	7.03	8.43	5.97
CO rate (mmol/(gcat h)	21.79	19.95	21.68	21.00	24.88	24.52	31.03	28.43	27.55	25.08
FTS rate (mmol/(gcat h)	11.97	10.82	13.65	13.32	15	14.97	18.42	17.58	16.57	14.97
CO_2 rate (mmol/(gcat h)	9.82	9.13	8.03	7.68	9.88	9.55	12.61	10.85	10.98	10.11
Carbon usage rate	0.55	0.54	0.63	0.63	0.60	0.61	0.60	0.62	0.60	0.60
Selectivity (mol%)										
CO_2	43.37	42.87	37.04	36.59	39.72	38.95	40.62	38.17	39.84	40.30
Hydrocarbons and oxygenates	56.63	57.13	62.96	6341	60.28	61.05	59.38	61.83	60.16	59.70
Oxygenates in oil (wt%)	16.33	17.98	21.93	22.33	22.02	23.33	22.85	23.13	22.07	22.29
HC distribution (wt%)										
C_1	7.49	8.15	6.06	5.46	7.95	8.39	8.05	8.06	6.40	6.52
C_2–C_4	17.50	18.83	26.22	26.76	24.31	24.88	23.65	23.11	17.58	18.42
$C_2^=$–$C_4^=$	9.73	11.34	13.68	14.62	14.05	15.60	14.26	14.46	9.77	10.74
C_5–C_{11}	19.75	21.75	22.87	24.26	24.99	25.49	27.06	29.02	29.44	30.66
C_{12}–C_{18}	26.00	25.27	21.16	21.22	20.22	19.28	20.12	19.24	25.16	25.31
C_{19}^+	29.26	26.00	23.68	22.29	22.54	21.96	21.12	20.57	21.41	19.09
$C_2^=$–$C_4^= + C_5^+$	84.74	84.36	81.39	82.39	81.80	82.33	82.57	83.28	85.79	85.80
Olefin selectivity										
$C_2^=$–$C_4^=/C_2$–C_4	0.56	0.60	0.52	0.55	0.58	0.62	0.60	0.63	0.56	0.58
$C_5^=$–$C_{11}^=/C_5$–C_{11}	0.51	0.54	0.50	0.51	0.53	0.57	0.55	0.58	0.52	0.53
Chain growth probability										
α_1*	0.72	0.71	0.70	0.69	0.70	0.69	0.69	0.68	0.68	0.68
α_2	0.88	0.87	0.85	0.84	0.85	0.84	0.84	0.83	0.84	0.83
Y_{ST} (C_5^+)[d] (g/mlcat h)	0.11	0.13	0.13	0.14	0.15	0.16	0.17	0.17	0.15	0.15
Y_{ST} (HC) (g/mlcat h)	0.16	0.17	0.16	0.15	0.19	0.18	0.21	0.19	0.18	0.16

[a] Time on stream (TOS, h).
[b] The ratio of H_2/CO usage.
[c] H_2/CO mole ratio in tail gas.
[d] Space time yield.
* α_1 and α_2 are growth probabilities in carbon number ranges of C_3–C_8 and C_{10}–C_{20}, respectively.

selectivity of olefins is observed. This indicates that appropriate amount of magnesium addition can improve the olefin selectivity, however, less or excessive magnesium addition will inhibit olefin formation. A monotonic increase from 19.75% to 30.66% in the selectivity of gasoline product (C_5–C_{11}) is observed with the increase of the magnesium content. The study of Gallegos et al. [13] found that the size of metal crystal and basicity of the support mainly influence the selectivity to olefins of the catalyst. In the present study, the catalyst incorporated with an optimal amount of MgO (Mg/Fe = 0.07) is the one which well controls the particle size and produces more olefins. The selectivity of diesel fuel product (C_{12}–C_{18}) first decreases, reach a minimum at the ratio of Mg/Fe = 0.07, and then increases. The selectivity of the high molecular hydrocarbon (C_{19}^+) monotonously decreases from 29.26% to 21.41% with the increase of the magnesium content. As shown in Table 6, the chain growth probabilities for catalysts with different magnesium content were calculated in carbon number range of C_3–C_8 and C_{10}–C_{20}. It is clear that the addition of magnesium slightly suppresses the chain growth ability of catalysts, and with the increase of the magnesium content chain growth probability α_1 and α_2 decrease from 0.72 to 0.68 and 0.88 to 0.84, respectively. Recently, Luo and Davis [10] compared group II alkali-earth metal-promoted iron-based catalysts with potassium-promoted and unpromoted catalysts for Fischer–Tropsch synthesis in a slurry reactor. The results showed that the catalysts promoted with magnesium have lower FTS activity and lower chain growth probability than the potassium-promoted iron catalyst, but higher activity and chain growth probability than unpromoted catalyst.

The space time yields of C_5^+ and of total hydrocarbon first increase with the increase of the magnesium content and reach a maximum at the Mg/Fe = 0.07. Then the decline of the space time yields of C_5^+ and of total hydrocarbon is observed. The selectivity of the effective hydrocarbon ($C_2^=$–$C_4^= + C_5^+$) of catalyst M-1 is lower than that of unpromoted catalyst, dropping from 84.5% drop to 81.5%. However, for the catalysts containing

magnesium, the selectivity of the effective hydrocarbon monotonously increase with the increase of the magnesium content. The selectivity of oxygenates in oil phase on the catalysts promoted with magnesium is obviously higher than that on the catalysts M-0, but the selectivities of oxygenates among the catalysts are similar to each other. Overall, the promoter of magnesium in the catalysts is an effective promoter to shift product selectivity to lighter molecular weight hydrocarbons and olefins, especially for gasoline products (C_5–C_{11}).

As shown here and in Table 6, the CO_2 selectivity of the catalyst M-0 is the highest among the five catalysts, but there is no obvious difference in the CO_2 selectivity among the magnesium-promoted catalysts. The decrease of CO_2 over Mg-promoted catalyst is due to the slight suppression effect of magnesium on the WGS reaction. It is well known that the CO conversion level has an important impact on relative activities of FTS and WGS over iron-based catalyst, resulting in different product selectivity values. As shown in Table 6, the rates of CO conversion of the catalysts M-0 and M-1 is similar to each other, but the rate of CO conversion over the magnesium-promoted catalysts increases with the increase of the magnesium content and reaches a maximum at the magnesium content of Mg/Fe = 0.07. Beyond this content the rate of CO conversion decreases with the further increase of the magnesium content. Since the CO conversion levels are different for all the magnesium-promoted catalysts, it is difficult to acquire a clear correlation between the content of magnesium and the selectivity of CO_2. The activity of FTS reaction of the catalysts with the magnesium promoter is higher than that of the catalyst without the magnesium promoter, and the change tendency of the FTS reaction rate on the Mg-promoted catalysts is similar to that of the CO conversion. The WGS reaction is a side-reaction accompanied with FTS. The CO can be converted to either hydrocarbon by FTS reaction or CO_2 via WGS reaction. The rate of CO_2 formation is equal to the rate of the WGS. As shown in Table 6, the carbon usage ratio (fraction of CO converted to hydrocarbons) of the catalysts with the magnesium promoter is higher than that of the catalyst without the magnesium promoter, but the carbon usage ratios of the catalysts with the magnesium promoter are similar to each other. The study of Luo and Davis [10] indicated that the addition of the magnesium promoter into the iron-based catalyst increases the carbon usage ratio. This is consistent with our results. The results of the CO_2 selectivity and the carbon usage ratio suggest that the addition of magnesium inhibits the WGS reaction.

4. Conclusions

The magnesium promoter for iron-based FTS catalysts was systemically studied in this work. Iron-based catalysts promoted with magnesium in the range of 0.02–0.11 (Mg/Fe) lead to smaller α-Fe_2O_3 crystallite sizes and higher BET surface areas. The addition of a certain level of magnesium promoter into the catalysts can promote the reduction and can accelerate the carburization of the catalysts, and enhance the dispersion of α-Fe_2O_3 and CuO. However, excessive magnesium addition will suppress this action. The contents of iron carbides in the activated catalysts first increase with the increase of the magnesium content and reach a maximum over the catalyst M-3, then decline. A maximum in catalytic activity (FTS) is obtained at a particular level of magnesium (Mg/Fe = 0.07), and there is a decline in activity at magnesium levels in excess amount.

Magnesium is an effective promoter to shift FTS selectivity to lighter molecular weight hydrocarbons, especially for gasoline product (C_5–C_{11}) and it suppresses the hydrogenation of light olefins ($C_2^=$–$C_4^=$), which causes the increase of light olefin content in the products. The space time yields of C_5^+ and of total hydrocarbon increase with the increase of the magnesium content, and pass through a maximum at the Mg/Fe = 0.07. After the maximum point, the space time yields of C_5^+ and total hydrocarbon decrease with further increase of the magnesium content. The effect of the magnesium promoter on the selectivity of oxygenates is not obvious. The catalyst M-3 is the best among the five catalysts. The catalyst M-3 has a high CO conversion of 90%, the selectivity to the total effective hydrocarbon ($C_2^=$–$C_4^=$ + C_5^+) of 83%, CH_4 selectivity of about 8%, and better stability during the whole course of the reaction.

Acknowledgements

We gratefully acknowledge financial support from the Chinese Academy of Sciences (Project No. KGC X1-SW-02) and National Ministry of Science and Technology of China via 863 plan (Project No. 2001AA523010).

References

[1] H.H. Storch, N. Golumbic, R.B. Anderson, The Fischer–Tropsch and Related Syntheses, John Wiley & Sons, New York, 1951.
[2] H. Pichler, Twenty-five years of synthesis of gasoline by catalytic conversion of carbon monoxide and hydrogen, in: W. Frankenburg, E. Rideal, V. Komarewsky (Eds.), Advances in Catalysis, vol. IV, Academic Press Inc., New York, 1952.
[3] R.B. Anderson, The Fischer–Tropsch Synthesis, Academic Press Inc., New York, 1984.
[4] T. Riedel, H. Schulz, G. Schaub, et al., Top. Catal. 26 (2003) 41.
[5] C. Maretto, R. Krishna, Catal. Today 66 (2001) 241.
[6] M.E. Dry, Catal. Today 71 (2002) 227.
[7] K. Jothimurugesan, J.G. Goodwin, S.K. Santosh, J.J. Spivey, Catal. Today 58 (2000) 335.
[8] Y.M. Jin, A.K. Datye, J. Catal. 196 (2000) 8.
[9] L. Guczi, P. Putanov, Stud. Surf. Sci. Catal. 61 (1991) 251.
[10] M.S. Luo, B.H. Davis, Appl. Catal. A: Gen. 246 (2003) 171.
[11] P. Putanov, G. Boskovic, L. Guczi, J. Mol. Catal. 71 (1992) 81.
[12] H. Kölbel, H. Giehring, Brennst.-Chem. 44 (1963) 343.
[13] N.G. Gallegos, A.M. Alvarez, M.V. Cagnoli, J.F. Bengoa, S.G. Marchetti, R.C. Mercader, A.A. Yeramian, et al., J. Catal. 161 (1996) 132.
[14] M.E. Dry, G.J. Oosthuizen, J. Catal. 15 (1969) 190.
[15] R. Dutartre, P. Bussière, J.A. Dalmon, G.A. Martin, J. Catal. 59 (1979) 382.
[16] P. Putanov, E. Kis, G. Boskovic, Appl. Catal. 73 (1991) 17.
[17] B.S. Wu, L. Bai, H.W. Xiang, Y.W. Li, Z.X. Zhang, B. Zhang, Fuel 83 (2004) 205.
[18] Y.Y. Ji, H.W. Xiang, J.L. Yang, Y.W. Li, B. Zhong, Appl. Catal. A: Gen. 214 (2001) 77.
[19] D.B. Bukur, M. Koranne, X. Lang, Appl. Catal. A: Gen. 126 (1995) 85.
[20] E.S. Lox, G.B. Marin, P. Bussiere, Appl. Catal A: Gen. 40 (1988) 197.
[21] R.J. O'Brien, L.G. Xu, R.L. Spicer, S.Q. Bao, D.R. Milburn, B.H. Davis, Catal. Today 36 (1997) 325.

[22] G.B. Raupp, W.N. Delgass, J. Catal. 58 (1979) 197.
[23] J.W. Niemantsverdriet, A.M. Van der Kraan, J. Phys. Chem. 89 (1985) 67.
[24] R.G. Robert, P. Jonathan, J. Catal. 104 (1978) 365.
[25] N. Sirmanothan, H.H. Hamdeh, Y. Zhang, B.H. Davis, Catal. Lett. 82 (2002) 191.
[26] Y. Yang, H.W. Xiang, Y.Y. Xu, L. Bai, Y.W. Li, Appl. Catal. A: Gen. 266 (2004) 181.
[27] S. Huang, L. Xu, B.H. Davis, Fuel Sci. Technol. Int. 11 (1993) 639.
[28] M.D. Shroff, D.S. Kalakkad, A.G. Sault, A.K. Datye, J. Catal. 156 (1995) 185.
[29] G. Bian, A. Oonuki, Y. Kobayashi, N. Koizumi, M. Yamada, Appl. Catal. A: Gen. 219 (2001) 13.
[30] F. Blanchard, J.P. Reymond, B. Pommier, S.T. Teichner, J. Mol. Catal. 17 (1982) 191.
[31] J.P. Reymond, P. Meriaudeau, S.J. Teichner, J. Catal. 75 (1982) 39.
[32] C.S. Kuivila, P.C. Stair, J.B. Butt, J. Catal. 118 (1989) 299.
[33] R.A. Dictor, A.T. Bell, J. Catal. 97 (1986) 121.
[34] T.R. Motjope, H.T. Dlamini, G.R. Hearne, N.J. Coville, Catal. Today 71 (2002) 335.
[35] L.D. Mansker, Y. Jin, D.B. Bukur, A.K. Datye, Appl. Catal. A: Gen. 186 (1999) 277.